Physical Modelling of High Speed Magnetic Bearing Systems

R. G. JOHNSON, D. PANG, J. A. KIRK AND D. K. ANAND

ABSTRACT

Magnetic bearings offer significant advantages due to their non-contact operation. Higher speeds, no friction, no lubrication, precise position control, and active damping make them far superior to mechanical bearings. The University of Maryland has developed a combination electro/permanent magnet bearing that axially supports a flywheel and provides active radial displacement control. A vertically stacked system integrates two bearings and a motor/generator for kinetic energy storage applications. The current aluminum flywheel is designed to rotate at 15 kRPM, with a composite follow-on reaching 80 kRPM and capable of storing 500 watt-hours.

Because of nonlinear effects, a closed solution analysis is practically impossible. Permeance modelling, empirical data, finite element analysis, and other numerical methods are generally used to determine the characteristics of such device. In the PM/EM bearing, high rotational speeds cause flywheel deformation and air gap growth. Gyroscopic effects and dynamic imbalance in the flywheel couples the two radial axis motion. Pole face misalignment due to the flywheel weight decreases axial stiffness. The cycling magnetic fields caused by flywheel rotation increases hysteresis and eddy current losses.

This paper discusses the physical modelling of nonlinear high-speed factors: dynamic motion, displacement sensor error, pole face misalignment, disturbance force, gyroscopic motion, and air gap growth. Part of the modelling includes a computer simulation of the bearing magnetic circuitry which analyzes nonlinear magnetic and geometric effects. The program functions as a design tool for future prototype development.

INTRODUCTION

The flywheel energy storage (FES) system [1] shown in Figure 1 relies on two magnetic bearings to suspend a flywheel against gravity and destabilizing radial forces. Because the bulk of magnetic flux is provided by permanent magnets, power

Department of Mechanical Engineering, University of Maryland, College Park, MD 20742 USA

requirements are reduced to that of a motor/generator for energy conversion and electromagnets for stabilization. The system's high efficiency, high specific energy density, and low environmental impact make it a more viable alternative to other forms of stored energy.

Limiting factors include material strength of the flywheel, torque generating capacity of the motor/generator, control system response frequency, and bearing force capabilities. The composite flywheel currently being developed will withstand speeds up to 80 kRPM and the motor/generator has been designed to commutate at that speed in the vacuum. The last two factors, however, are more difficult to assess when considering high-speed operation.

A block diagram of the bearing operation is shown in Figure 2. Voltage feedback from the control system is combined with disturbance force F_d and sensor noise η. The actuator consists of the power amplifier and electromagnets, which provide additional flux in the air gap where needed to stabilize the bearing. Rotor dynamics results from the rotational inertia and the destabilizing radial force from the permanent magnet flux distribution.

DISTURBANCE CONSIDERATIONS

A single magnetic bearing system has four centers: geometric center, mass center, magnetic center and sensor center. Ideally, the four centers are coincident. Eccentric errors will introduce disturbances into the system. We assume the rotor is a geometrically perfect cylinder. The eccentric errors of the other centers will cause a mass imbalance, magnetic imbalance, and sensor error. At low speed the magnetic bearing will force the rotor to spin at the sensor center. At high speed the rotor will spin along the inertia axis. A mass imbalance is caused by the rotation of an eccentric mass. The imbalance force can be written as

$$F_{du} = Md_u\Omega^2 e^{j\Omega t} \tag{1}$$

where d_u is the distance between the mass center and the rotating center, and Ω is the rotating speed.

The magnetic imbalance due to uneven magnetic flux distribution in the air gaps of the magnetic bearing will cause a fluctuating force even at very low speed of

$$F_{dm} = K_a d_m e^{j\Omega t} \tag{2}$$

where K_a is the active stiffness of the magnetic bearing, and d_m is the distance between the magnetic center and the rotating center.

The sensor center is the intersection of two axes of the displacement sensors, which maintain an uniform gap to the rotor. The sensor error can be represented as

$$\eta = d_s e^{j\Omega t} \tag{3}$$

where d_s is the distance between the sensor center and the rotating center.

Errors will be further compound by imperfect geometries of the bearing and

rotor components and an axial misalignment between pole faces of the stator and rotor. Because the FES system consists of two magnetic bearings and a motor/generator it becomes very difficult to experimentally differentiate between error sources.

ROTOR DYNAMICS

The rotor dynamic modelling includes the mechanical dynamic behavior of the stator and rotor with their inherent destablizing force from the permanent magnets. Lashley et. al. [2] conducted a model test of a four inch prototype aluminum flywheel system. An impact test of the freely suspended flywheel shows its first natural frequency is 4.35 kHz. Because this value is substantially above the maximum operating speeds (1.33 kHz), rigid body motion analysis is valid. The support structure has four natural frequencies below the maximum operating speed, but it is feasible to alter the dynamic characteristics via the structural design. For a proposed composite flywheel the first natural frequency is calculated to be 2.14 kHz, which is also above the maximum operating speed.

For a single magnetic bearing the rotor dynamics can be viewed as planar motion, a problem with two degrees of freedom. Because of axis symmetry, the rotor dynamics can be further simplified to be one degree of freedom problem. The dynamic equation becomes

$$M\ddot{x}-K_x x=-F_c+F_d \tag{4}$$

where F_c and F_d are the corrective and disturbance forces.

The flywheel spins on the Z axis at a rate of Ω rad/s. The flywheel has four degrees of freedom, X_1, X_2, Y_1 and Y_2, which are the displacements of the flywheel measured at the magnetic bearing planes. The dynamic equations of gyroscopic effects show X and Y coupled at high speed:

$$\begin{aligned}
&\frac{M(\ddot{x}_1+\ddot{x}_2)}{2}-K_x(x_1+x_2)=-(F_{cx1}+F_{cx2})+(F_{dx1}+F_{dx2})\\
&\frac{M(\ddot{y}_1+\ddot{y}_2)}{2}-K_x(y_1+y_2)=-(F_{cy1}+F_{cy2})+(F_{dy1}+F_{dy2})\\
&\frac{J_x(\ddot{y}_2-\ddot{y}_1)}{2l}+\frac{J_z\Omega(\dot{x}_1-\dot{x}_2)}{2l}-K_x(y_2-y_1)l=-(F_{cy2}-F_{cy1})l+(F_{dy2}-F_{dy1})l\\
&\frac{J_x(\ddot{x}_1-\ddot{x}_2)}{2l}-\frac{J_z\Omega(\dot{y}_2-\dot{y}_1)}{2l}-K_x(x_1-x_2)l=-(F_{cx1}-F_{cx2})l+(F_{dx1}-F_{dx2})l
\end{aligned} \tag{5}$$

where l is the distance between the flywheel center of mass and the magnetic bearing plane; F_{cx1}, F_{cx2}, F_{cy1}, and F_{cy2} are the corrective forces; and F_{dx1}, F_{dx2}, F_{dy1}, and F_{dy2} are the disturbance forces. The first two dynamic equations are translational motions of the flywheel and the last two equations are the rotating motions.

MAGNETIC CIRCUIT ANALYSIS

Figure 3 shows a simplified magnetic circuit of one axis of the bearing. The samarium-cobalt permanent magnet behaves linearly due to its high intrinsic coercivity, and can be simulated as a magnetomotive force ($B_rA_mR_m$) with an internal reluctance R_m. The four electromagnets are connected in parallel to the power amplifier, where the magnetomotive force of each electromagnet is ($Ni_c/4$). The reluctance of the core material is first considered negligible compared to the reluctances of the air gap and leakage paths, R_g and R_L, where

$$R_g=\frac{2g}{\mu_o A_g} \tag{6}$$

The bias flux B_u generated by the permanent magnet across the air gap is

$$B_u = \frac{B_r A_m}{A_g} \quad \frac{R_m R_L}{R_m R_L + R_g R_m + R_L R_g} \tag{7}$$

The flux density B_{EM} generated by the electromagnets across the air gap is

$$B_{EM}=\frac{Ni_c}{2R_g A_g} \tag{8}$$

If we assume the air gap is increased from its nominal value g_o to $(1+\delta)g_o$ where δ is the gap growth factor, the reluctance of the useful flux will become $(1+\delta)R_g$. The reluctance of the leakage flux is unchanged because the major leakage flux in the bearing is between the two bias plates. The bias flux density B_u and the EM flux density B_{EM} becomes

$$B_u=\frac{B_{uo}}{1+\alpha\delta} \tag{9}$$

$$B_{EM}=\frac{B_{EMo}}{1+\delta} \tag{10}$$

where $\alpha = (R_LR_g + R_gR_m)/(R_LR_g + R_gR_m + R_mR_L)$. α is less than unity for any circuit containing a permanent magnet, and is approximately 0.75 for the UM bearing. B_{uo} and B_{EMo} are the B_u and B_{EM} values at zero displacement. To stabilize the rotor the control system will generate a current through the EM coils. The EM flux will be added in the larger air gap side and be subtracted from the small air gap side. The combined restoring force F_{rad} of the magnetic bearing is

$$F_{rad}=\frac{A_g}{2\mu_o}\left[\left(\frac{B_{uo}}{1+\alpha\delta}+\frac{B_{EMo}}{1+\delta}\right)^2-\left(\frac{B_{uo}}{1-\alpha\delta}-\frac{B_{EMo}}{1-\delta}\right)^2\right] \tag{11}$$

If the magnetic bearing is operated near the center and the current is small, the

combined restoring force becomes

$$F_{rad}=\frac{B_{uo}A_gN}{2g_o}i_c-\frac{2\alpha B_{uo}^2A_g}{\mu_o g_o}x=K_i i_c-K_x x \tag{12}$$

The force F_{rad} can also be represented by two magnetic characteristics: the passive radial stiffness, K_x, and force/current sensitivity, K_i.

$$K_x=\frac{2\alpha B_{uo}^2A_g}{\mu_o g_o}$$
$$K_i=\frac{B_{uo}A_gN}{2g_o} \tag{13}$$

GAP GROWTH EFFECTS

In the FES application, the flywheel is designed to rotate between 40 and 80 kRPM. At these speed the flywheel experiences stress which causes outward deformation of the flywheel. The air gap is increased between the bearing and the return ring of the flywheel. It has been estimated the gap growth is varied between 4 and 16 mils (0.102 and 0.406 mm) comparing to the nominal gap of 40 mils (1.016 mm) [2]. The gap growth will change the magnetic characteristics such as K_x and K_i. For a gap growth factor δ

$$K_x=\frac{K_{xo}}{(1+\alpha\delta)^2(1+\delta)}$$
$$K_i=\frac{K_{io}}{(1+\alpha\delta)(1+\delta)} \tag{14}$$

where K_{xo} and K_{io} are the K_x and K_i values at zero speed.

NONLINEAR PERMEABILITY, HYSTERESIS, AND EDDY CURRENT EFFECTS

The permeability of the magnetic material is affected by the flux density (or magnetizing force), material thickness, manufacturing process, heat treatment and operating frequency. Figure 4 shows a computer-mapped μ-H curve of Carpenter steel 48% nickel iron used in the UM bearing. The permeability is nonlinear and drops dramatically when the magnetic material is operated near its magnetic saturation value. The permeability also decreases with higher operating frequencies due to eddy current generation. If the magnetic material has a significantly low permeability, its reluctance should then be included in the magnetic circuit analysis.

Hysteresis effect is the material shows a irreversible nonlinear multi-valued

behavior in the B-H curve when applied a sinusoid magnetizing force. The UM bearing uses a 48% nickel-iron alloy whose hysteresis losses are negligible compared to eddy current losses.

Eddy currents are generated when the conducting core material is subject to a time varying magnetic field. The first of these comes from the flywheel rotation which sweeps through the magnetic flux distribution beyond the stator. Secondly, the magnetic bearing control system generates a varying magnetic flux which centers the rotor in the radial direction. The overall effect is to lower the core permeability and the flux across the air gap, and generate heat in the magnetic material. The eddy current also generates a counter torque against the rotation and influences the transient response of the actuator. Zmood et. al. [3] derived a first order model of the eddy current effect in the radial direction.

COMPUTER-AIDED ANALYSIS

In order to determine bearing behavior in the axial direction a more detailed magnetic circuit was developed that included fringing paths around the air gap, leakage components, and finite element meshing of ferromagnetic regions. The Active Magnetic Bearing Evaluation Routine (AMBER) [4] takes input from data files or user entry of geometry, permanent magnet strength, control current settings, and ferromagnetic material permeability polynomial or exponential functions. It iteratively find the flux and flux density distributions in the network of over five hundred fixed and variable reluctance based on Kirchhoff's principles. An inertial permeability is assumed in all core parts of the bearing. Based on the reluctances established by the mean path lengths, cross-sectional areas, and permeabilities, the flux through each path is calculated. The resulting flux density is substituted into the material permeability curve polynomial, and a second permeability is determined. The adjusted permeability is calculated with a blending factor that auto-detects convergence or divergence of the cumulative errors and increases its own value.

The circuit is solved over a range of incremental axial pole face misalignments, representing axial drop due to flywheel weight. The coenergy of the magnetic field in the air gap region is calculated for each Z value, and the data pairs are curve-fit via linear regression with a fifth-order polynomial.

$$W'_{fld} = \int_{vol} \frac{B^2}{2\mu} = \sum_{n=1}^{\#\ regions} \frac{\phi_n^2 R_n}{2} \qquad (15)$$

The first derivative of this function with respect to the Z direction yields the axial force, and the second derivative yields the axial stiffness K_z.

The three material permeability curves in Figure 5 are programmed: DC, 60 Hz, and 400 Hz (corresponding to 0, 3600, and 24000 RPM) to represent the eddy current effects in the core material. The flywheel speed determine which two curves to interpolate between, as well as setting the gap growth factor due to centripetal forces. The bearing's maximum axial support can thus be fixed from geometry and speed.

Axial force error between experimental data and simulation results ranges between 0.2 and 3.0 lb (0.9 and 13.3 N) on the low side so it provides for a margin of

safety. Figure 6 illustrates a comparison of the theoretical and experimental axial force for the current bearing. The axial stiffness Kz ranges from over 300 lb/in (52.5 N/mm) near zero displacement, decreasing to 200 lb/in (35.0 N/mm) farther down. It is desired that the misalignment be no more than 20% of the pole face thickness, which corresponds to 0.024 in (0.61 mm).

CONCLUSION

This paper presents a physical model of the magnetic bearing system for high speed applications. The FES system becomes nonlinear due to gyroscopic motion, air gap growth, pole face misalignment, nonlinear permeability, and eddy current effects. The model includes these nonlinear factors as well as system disturbances such as eccentric mass, magnetic imbalance forces, and displacement sensor error. To analyze the nonlinear effects on the bearing computer simulation software called AMBER has been developed. AMBER applies magnetic circuitry, finite element analysis, and a coenergy method to calculate bearing axial force and stiffness. There is good correlation between simulation results and experimental data from existing bearings.

REFERENCES

1. Anand, D. K., Kirk, J. A., Iwaskiw, P., "Magnetically Suspended Stacks for Inertial Energy Storage Flywheel", Proceeding of 22th IECEC, 1987.
2. Lashley, C.M., Ries, D.M., Zmood, R.B., Kirk, J.A., Anand, D.K., "Dynamics Considerations for a Magnetically Suspended Flywheel", Proceeding of 24th IECEC, 1989.
3. Zmood R.B., Anand, D.K., Kirk, J.A., "The Influence of Eddy Currents on Magnetic Actuator Performance", Proceedings of IEEE, Vol. 75, No. 2, February 1987.
4. Johnson, R.G., Computer-Aided Modelling and Simulation of a Magnetic Bearing System, M.S.Thesis, University of Maryland, College Park, 1991.

NOMENCLATURE

α	flux density correcting factor
A_g	air gap pole face cross-sectional area
A_m	permanent magnet cross-sectional area
B_r	permanent magnet remanence
i_c	control system-induced EM current
J	mass moment of inertia
N	number of electromagnet coils
R_m	permanent magnet reluctance
μ_o	permeability of free space

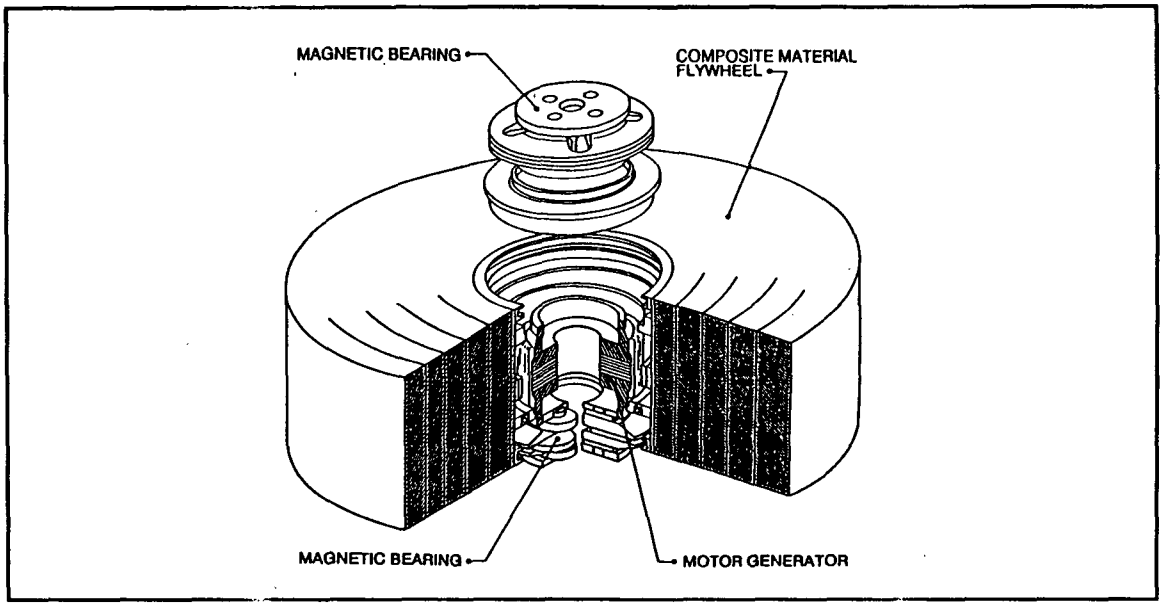

Figure 1 Flywheel Energy Storage System

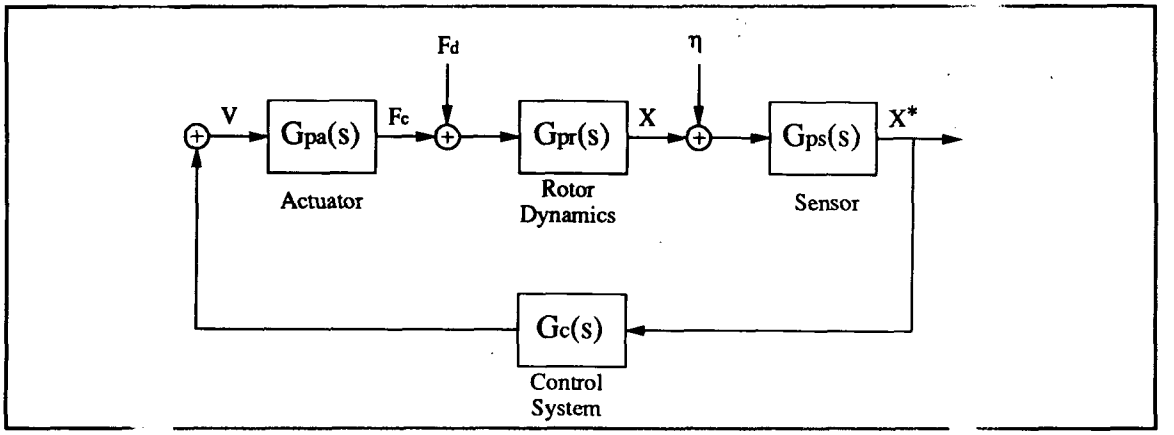

Figure 2 System Block Diagram

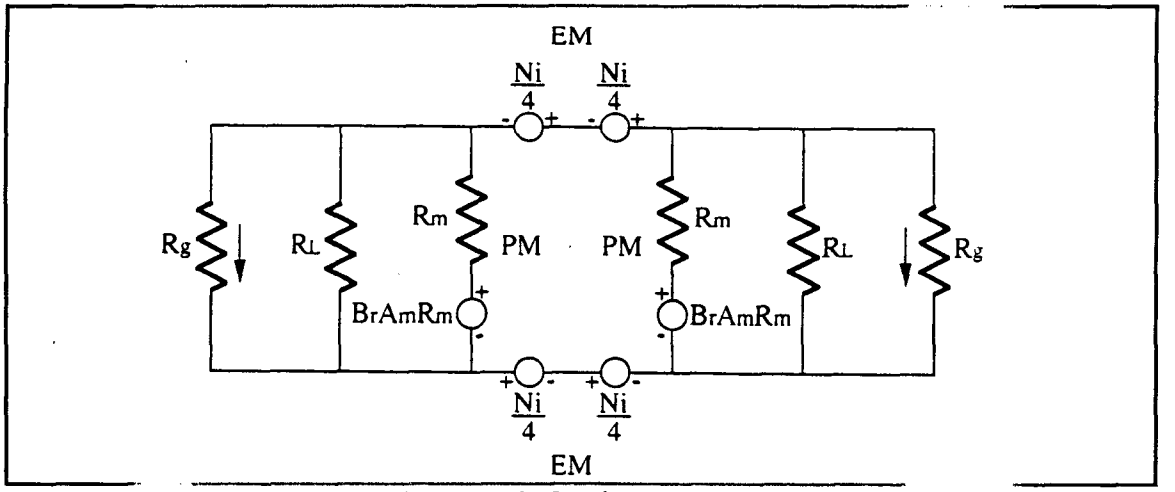

Figure 3 Magnetic Bearing Electrical Analog

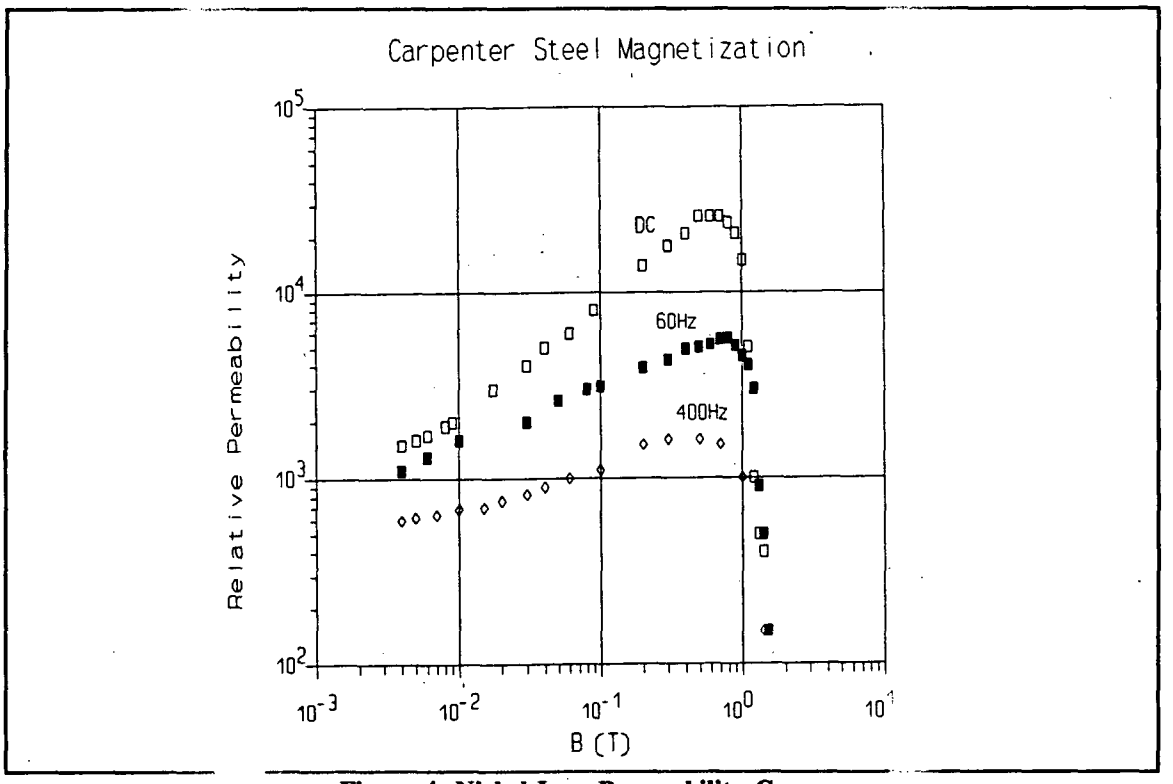

Figure 4 Nickel-Iron Permeability Curve

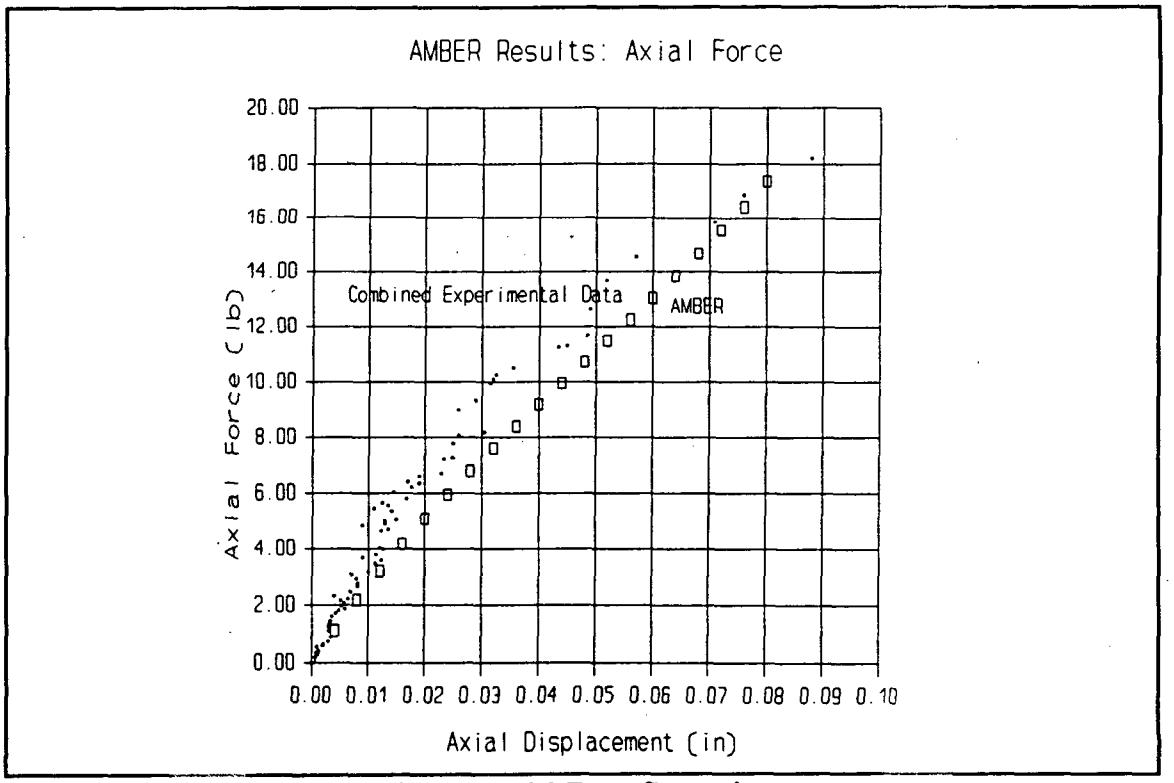

Figure 5 Axial Force Comparison